

Gravity wave–induced perturbations in marine stratocumulus

G. Allen¹, G. Vaughan¹, T. Toniazzo² H. Coe¹, P. Connolly¹, S. Yuter³, C. D. Burleyson³ P. Minnis⁴, J. K. Ayers⁴

[1]{Centre for Atmospheric Science, University of Manchester, UK}

[2]{Dept. of Meteorology, University of Reading, UK}

[3]{Dept. of Marine, Earth and Atmospheric Sciences North Carolina State University, USA}

[4]{NASA Langley NASA Langley Research Center, USA}

Abstract

We discuss the role of atmospheric gravity waves in modulating cloud radiative and dynamical properties over the South East Pacific. Satellite imagery and satellite-retrieved cloud properties during October 2008 illustrate three distinct episodes of horizontal propagation of gravity wave trains across the large-scale stratocumulus cloud deck capping the local marine boundary layer. In one period, 7-9 October 2008, the waves modulated cloud-top-height by over 500m peak-to-trough, propagating perpendicular to the synoptic boundary layer flow with phase speed 15.3ms^{-1} , period ~ 1 -hour and horizontal wavelength 55km. The gravity waves were observed to be non-dispersive. These waves were first evident in the cloud deck near 30°S , 85°W during a 24-hour period beginning at midday on 7 October 2008, and propagated northeastward toward the Peruvian coast for the following 48 hours. During this time, they induced both reversible and non-reversible changes in cloud-radiative and cloud-dynamic properties, such that areas of clear sky developed in the troughs of passing wavefronts. These pockets of open cells persisted long after the passage of the gravity waves, advecting northwestward with the background wind. Using ECMWF analysis fields in conjunction with infrared and microwave satellite imagery, we show that the gravity waves

observed during all three episodes emerged from a disturbed sub-tropical jet-stream. The radiant of the waves was coincident in all cases with centres of large negative residuals in nonlinear balance, suggesting that geostrophic readjustment of sharply divergent flows associated with the disturbed jet provided a source for the wave energy. Conversely, gravity waves were not observed in more quiescent jet conditions. This case study highlights the important and irreversible effects that gravity waves propagating in the troposphere can have on cloud radiative properties (and hence surface radiation budgets) over a very wide area. It also highlights the importance of synoptic influence on stratocumulus covered marine boundary layers.

Keywords: VOCALS, Stratocumulus, Gravity waves, pockets of open cells, cloud microphysics, scale interactions.

1. Introduction

The extensive stratocumulus sheets found in the subtropics on the eastern sides of the Pacific and Atlantic oceanic basins play an important role in the Earth's radiation budget through their high reflectivity. According to the Intergovernmental Panel on Climate Change, predicting how these, and other low clouds, will evolve in the changing climate of the coming centuries is one of the largest sources of uncertainty in current climate models (e.g. Randall et al., 2007; Meehl et al., 2007). One of the distinctive features of the stratocumulus sheets that cannot be reproduced in such models is the extensive dynamical variability, exemplified by the opening up of Pockets of Open Cells (POCs) in an otherwise-unbroken boundary-layer cloud. Understanding the physics of these POCs was one of the main objectives of the VOCALS experiment (see below) conducted in the South-East Pacific in the (southern) spring of 2008. Here we report on a possible trigger for the formation of these features by atmospheric gravity waves propagating across the domain of the cloud sheet. This paper also shows how reversible dynamical perturbations caused by gravity waves can, through their interaction with the cloud microphysics, result in irreversible changes in the cloud field.

The processes responsible for POC formation are believed to involve a coupling between cloud microphysics, aerosols and boundary-layer dynamics (e.g. Wood et al., 2011a, Bretherton et al., 2004; Stevens et al., 2005; Comstock et al., 2004, and references therein). Very briefly, local dynamical processes leading to enhanced drizzle formation in stratocumulus clouds remove moisture and cloud condensation nuclei (CCN) from the boundary layer, thus suppressing recovery of the cloud from the moisture sink of drizzle. A range of both modelling (e.g. Wang et al., 2010) and observational case studies (Stevens et al., 2005; Comstock et al., 2007; and Wood et al., 2011a) of marine Sc have now linked the formation of POCs with the presence of drizzle in a CCN-poor environment. Ship observations during VOCALS-Rex (see Section 2.1) consistently showed more intense clouds and drizzle and higher LWP when cloud tops were higher (deSzoek et al. 2010). In a modelling study of the area near 20°S, 85°W, where strong drizzle was observed during

VOCALS, Mechem et al. (2001) found that an increase in the boundary layer height of 200 m yielded a greater change in drizzle intensity than halving CCN concentration from 270 cm^{-3} to 135 cm^{-3} . When the cloud passes a critical (as yet uncharacterised) threshold in terms of CCN concentration and bulk properties such as liquid water content, it dissipates and responds dynamically by switching from closed cellular to open cellular convection with the remaining cloud limited to the ascending branches of the open cells.

The hypothesis being examined here is that a gravity wave imposes a periodic pattern of vertical motion on the cloud deck, alternately lifting and lowering it. As the cloud is lifted it thickens and cools, causing drizzle to form which washes out moisture and CCN. In the opposite phase of the wave the cloud warms and dissipates, creating a hole. When the wave has passed, this hole is left behind as a nascent POC.

Whilst earlier studies have demonstrated a potential coupling between tropospheric gravity wave generation and relatively short-lived cloud formation (lasting a few hours at most) through dynamical arguments alone (e.g. Knippertz et al., 2010; Haag and Karcher., 2004), the process discussed in this study suggests a hitherto unidentified role for gravity waves through both long-range and long-lived influences on tropospheric cloud. Furthermore, this study suggests a coupling to irreversible microphysical processes, which, under appropriate conditions, may lead to cloud destruction, with consequences for the tropospheric energy budget and hence climate.

In this paper, we will examine satellite imagery and thermodynamic fields for October 2008, focusing in detail on the period 7 to 9 October, when gravity waves were observed to have the most pronounced impacts on cloud properties. We will then briefly discuss two other episodes of gravity wave propagation which reveal a common source mechanism. We now briefly describe the field project that was active at the time of interest to the case study and describe our data sources before continuing to discuss satellite and thermodynamic observations.

2. The VOCALS campaign and data sources

2.1 The VOCALS-REx Campaign

The events discussed here were observed immediately prior to the intensive phase of the Variability in the American Monsoon System (VAMOS) Ocean Atmosphere Land Study Regional Experiment (VOCALS-REx) field campaign, and we make use of satellite data generated in support of this international multi-platform campaign. A key objective of VOCALS-REx was to reduce uncertainties in current and future climate projections; especially those associated with marine stratocumulus and coupled land-ocean-atmosphere processes. The field campaign consisted of the following measurement platforms: five aircraft, two cruise ships, two surface measurement sites and data from two IMET Buoys (positioned at 20°S, 85°W; and 20°S, 75°W) as well as a host of supporting satellite data and specialist model output to inform mission planning in the field. Further details of the context, platforms and instrumentation operated during VOCALS-REx can be found in Wood et al. (2011b), Allen et al. (2011), and Bretherton et al. (2009).

2.2 Satellite datasets

Satellite measurements provide a practical method for observing marine stratocumulus (hereafter Sc) and cloud bulk properties over the remote open ocean. In this study, we make use of visible, infrared and microwave satellite spectroradiometers, which include the 10th Geostationary Operational Environmental Satellite (GOES-10); and the MODerate-resolution Spectroradiometer (MODIS) and Advanced Microwave Sounding Radiometer-EOS (AMS-R-E) on NASA's polar-orbiting Aqua satellite

The GOES-10 geostationary weather satellite, jointly operated by NOAA and NASA, routinely provided infrared and visible images of the South American region from 1997 until its decommissioning in 2009 (see Menzel and Putdom, 1994, for further technical details). The GOES-10 recorded 4-km resolution images in five spectral bands including a visible, shortwave infrared and three thermal infrared channels. For this work we use half-hourly brightness temperatures recorded in the GOES-10 infrared window (IRW) channel 4 (10.8 μm) to illustrate the propagation

of gravity waves. This mid-infrared channel is chosen to limit sensitivity to changes in cloud top radiance inherent to the diurnal cycle. Brightness temperature perturbations are used as a proxy for changes in cloud top temperature and hence cloud top height. In addition, cloud properties were retrieved from GOES-10 imagery at half-hourly intervals, using the Visible Infrared Solar-Infrared Split Window Technique (VISST) and the Solar-Infrared Split Window Technique (SIST) methods described by Minnis et al. (2011). These methods use GOES-10 brightness temperatures in four channels during daytime (VISST) and three during night-time (SIST) in conjunction with other available satellite and meteorological observations to derive information on cloud top height (CTH), liquid water path and other bulk cloud quantities. CTH is defined as the point of least difference between cloud top temperature and a co-located ECMWF reanalysis temperature profile.

Data from both the MODIS and AMSR-E sensors are used here to detect strong drizzle. Drizzle forming in the presence of the gravity waves (see Section 3) is identified using a novel technique (Miller and Yutter, 2011). There were eleven Aqua overpasses of the southeast Pacific (SEP) region between October 7th and 10th 2008, occurring approximately half an hour after local noon and midnight.

In clouds without ice, such as the marine Sc in the South East Pacific, strong drizzle ($LWP > 200 \text{ g m}^{-2}$) manifests as small patches of higher microwave brightness temperatures when contrasted with the smoother background emission from the ocean surface and water vapour. The AMSR-E 89-GHz brightness temperatures are used to detect drizzle at the native resolution of the sensor (4 km x 6 km) which is sufficient to identify larger regions of strong drizzle. The method works only in regions without mixed phase or ice clouds and where the drizzle is strong. Hence, this technique is well-suited for this study, where most often, only Sc clouds appear in the field-of-view over the South East Pacific.

2.3 ECMWF reanalysis data

For synoptic meteorological analysis, we use operational analysis fields produced by the European Centre for Medium Range Weather Forecasting (ECMWF) Integrated Forecasting System (IFS Cycle 29r2) on a $2.5^\circ \times 2.5^\circ$ geospatial grid on 91 hybrid model levels. Derived variables such as potential vorticity are calculated explicitly here from base thermodynamic fields (pressure, temperature, specific humidity and 3-dimensional winds).

In addition, for the purposes of this study, we will use base thermodynamic fields to diagnose a spatially gridded residual to the nonlinear balance equation (NBE) as a proxy for regions of unbalanced flow associated with large curvature in high amplitude Rossby waves, which were known to be prevalent over the South East Pacific in October 2008 (Toniazzi et al., 2011). The residual to the NBE is defined as (e.g. Zdunokowski and Bott, 2003, p. 450):

$$\Delta NBE = 2J(u, v) + f\zeta - \nabla^2\Phi - \beta u \quad (1)$$

Where f is the Coriolis frequency, $\beta = df/dy$, ζ is relative vorticity, Φ is geopotential height and the Jacobian term, $J(u, v) = (du/dx \cdot dv/dy) - (dv/dx \cdot du/dy)$. The NBE is obtained through scale analysis of the divergence equation by dropping all terms containing the divergence and the vertical velocity. A nonzero-sum of the terms of the r.h.s. of (1) has previously been shown to represent flow imbalance associated with strong divergence seen in rawinsonde data (Moore and Abeling, 1988) and has also been employed with mesoscale model fields for the purpose of analysing the degree of flow imbalance. Most importantly, in those studies (Zhang et al., 2001; Zack and Kaplan 1987; Koch and O'Handley 1997; Koch et al. 1998) a region of large NBE residual was found to occur within the generation region of gravity waves.

3 Observations from satellite imagery between 7 October and 9 October 2008

We now focus on the period 7 October to 9 October 2008 when gravity waves were observed to cause the largest modulation of cloud top height over the South East Pacific. Figure 1 shows a time sequence of GOES-10 IRW brightness temperature maps grey-scaled within the range 277 K to 283

K for a period between 05:45 local time (08:45 UTC) on 8 October 2008 and 13:45 local time (16:45 UTC) on 9 October 2008. Yellow areas on this scale indicate brightness temperatures less than 250 K and hence high level cirrus. The sequence shows several parallel wave fronts superimposed on the brightness temperature field, evident as light and dark bands aligned roughly in a northwest/southeast direction between 90°W to 80°W; and 23°S to 27°S. White ellipses in Figure 1 highlight the wave fronts. Magnified images of the areas around the ellipses shown in Figure 1 are shown in Figure 2 with an approximate spatial scale (assuming Great Circle distance at 20 S) and serve to better illustrate the individual wave fronts. The sequence shows that the wave front seen in Figure 1a advanced toward the northeast and was the first wave front of a wave train. A more detailed tracing of each wave front from a full sequence of GOES-10 imagery reveals that the peak of each wave front propagated at a phase speed of approximately 55 km hr⁻¹ (15.3 m s⁻¹) across the domain. Furthermore, analysis of the inter-arrival time between these fronts at a fixed location yields a wave period of approximately 60 minutes and hence a wavelength of 55 km.

An important additional observation is that the waves were non-dispersive: there was no evidence of wave fronts propagating within a broader envelope moving at a different velocity. This is to say that the observed phase speed and group speed of were equal, which, as we argue below, has implications for the vertical structure of the waves. Figures 1(i-l) and Figures 2(i-l) show the sequence between 0445 UTC and 1645 UTC on 9 October, which completes the life cycle of the waves as they finally reach the Peruvian Coast at approximately 1645 UTC. We continue to track the POC feature of Figure 1f in the purple ellipse, demonstrating its northwestward advection and continued separation from the gravity wave train. By the end of the sequence, the POC feature, originally initiated well to the south east, had persisted for 28 hours before entering a more general cloud-free area to the west (in the transition region to trade cumulus outside of the Walker anticyclone). A composite schematic of the time and location of the foremost wave front observed in the GOES-10 imagery in Figure 1a is presented in Figure 3.

The light and dark banding in brightness temperatures seen in Figures 1 and 2 can be thought of qualitatively as peaks and troughs in cloud top temperature and hence troughs and peaks in cloud top height (CTH), respectively. Where solar zenith angle permitted GOES-10 CTH retrievals, we observe that the maximum peak-to-trough difference in cloud top height was 500 m (see Figure 4), around a mean CTH of ~1300 m at 20° S, 76° W. These periodic undulations in cloud top height also propagated almost perpendicular to the mean boundary layer flow (diagnosed from the ECMWF horizontal boundary layer wind field). This is observed in Figure 1 by the separation of the white and purple ellipses across the sequence, which track the gravity wave train and a resulting POC feature, respectively.

The sequence in Figure 1 shows that in a 32 hour period, the wave fronts propagated across approximately 10 degrees of longitude and 8 degrees of latitude over the South East Pacific northeastward toward the coast of Peru. A full animated sequence of GOES IRW brightness temperature imagery across October 2008 is provided as a supplement to this paper and should be viewed to better illustrate the propagation of the waves across the cloud deck. The nature of this periodic, cross-flow propagating disturbance, the phase speed and horizontal wavelength all point to a mesoscale gravity wave that was initiated to the southwest and travelled across the domain. We note that at the southernmost end of the domain the wave signature could also be seen in the cirrus clouds, showing that the gravity wave was present throughout the troposphere. A false-colour image of brightness temperature tuned for cirrus is presented in Figure 5. In this figure, we see a thin band of cirrus propagating over a 1.5-hour period beginning at 0828 UTC on 9 October 2008. The cirrus band is again aligned in a southeast-northwest direction and calculations of phase speed and period for the band seen across Figure 5 reveal values (phase speed 16.5 ms^{-1} , period 59 km) similar to the wave train observed a little to the north in the Sc deck below.

Figure 6 shows liquid water path (LWP) retrieved from GOES-10 radiances during the period of interest. It should be noted that accurate LWP estimates are not possible for high solar zenith angles ($>72^\circ$) due to the difficulty in accurately retrieving cloud effective radius, which requires

information from near-infrared channels and hence sunlight. We see a characteristic increase in LWP with distance offshore from the South American coast, a consistent feature described by George et al., 2010 (and references therein). These LWP changes are likely a result of the increasing depth of the boundary layer and changes in its structure further offshore (Bretherton et al., 2010). There is also a decreasing gradient in cloud droplet number away from the coast which is associated with atmospheric composition in the local marine boundary layer, in particular the presence (or absence) of sub-micron aerosol which act as cloud condensation nuclei (CCN) (Allen et al., 2011). Rain rate in Sc has been empirically observed to be proportional to the ratio of cloud liquid water path and droplet number (e.g. ship-based measurements reported by Comstock et al., 2004), meaning that rain rate increases with increasing LWP and decreasing droplet number. This relationship implies that there are both anthropogenic and natural influences on the observed precipitation rates across the region. Finer-scale variability in LWP in the South East Pacific has also been correlated with both precipitation and CCN number, with local increases in LWP, particularly in the remote marine environment, being coincident with areas of strong drizzle and low CCN (Zuidema et al., 2005). From those measurements and known relationships, we can conclude that stratocumulus clouds observed to contain relatively high LWP in the remote marine environment are more frequently precipitating than those with lower LWP near to shore

Figure 6a shows the crests of the gravity wave train at 2045 UTC on 8 October 2008 discussed earlier and seen in Figures 1 and 2, seen here as an increase in LWP relative to the background. The LWP along the wave fronts in Figure 3a is typically around 130 gm^2 compared to a background of around 80 gm^2 in the remote marine environment. One hour later, in Figure 6b, we can see that the wave train has advanced to the north-east and that a large area of enhanced LWP has developed as several more waves pass through the region. It is important to note that we expect a significant diurnal modulation in LWP and therefore the enhancements seen here should be interpreted in the context of the contrast between the wave crests and the instantaneous background. With this in mind, it is clear that the passing waves do enhance LWP relative to the unperturbed background.

Furthermore, in Figure 6b, we see the area of POCs corresponding to those observed in Figure 1f, seen here as areas of zero LWP embedded in the region of wave-enhanced LWP.

As discussed in Section 1, POCs are known to be associated with strongly drizzling Sc cloud, and hence enhanced LWP, relative to non-precipitating cloud in an otherwise similar airmass. Figure 7 shows detected drizzle cells from MODIS and AMSR-E overpasses using the method described in Section 2.2. Due to the short time period considered here, only a single overpass of the region was sampled by AMSR-E, at 0528 UTC on 9 October 2008 (Figure 7b), corresponding most closely with the GOES-10 images shown in Figures 1j and 2j. Figure 7b demonstrates that the wave crests seen at 18°S, 77°W in Figure 1j are indeed inducing precipitation at the same location sampled by AMSR-E, seen as the dark bands in the right panel of Figure 7b. For contrast, an earlier overpass at 0540 UTC on 7 October 2008, before the gravity waves were first observed, is plotted in Figure 7a, which shows an absence of significant drizzle across the region, with the exception of a small region of POCs near 24° S, 81 ° W.

In addition to influences on SCu cloud far offshore, there were also some noteworthy changes in the cloud field where the gravity wave train reached the near-shore environment, seen in terms of brightness temperature in Figures 1L and 2L, and in terms of LWP in Figure 6c. In particular, a large area of POCs located just to the south of a sharp gradient in LWP at around 18°S, 77°W (see Figure 2l), rapidly developed as the wave fronts passed through. The sharp gradient defines a natural boundary between the relatively clean maritime air and the more polluted coastal aerosol regime, bounded by the synoptic coastal jet – a dynamical feature associated with the Andes topography (see Rahn et al., 2011). Further linear bands of cloud clearance were also observed nearer to the coast. The reason for the rapid development of a POC feature at this location is unknown although we speculate that this could be due to a complex interaction between the propagating wave train and the coastal jet, which may be further underpinned by the rapid change in the aerosol regime. A detailed examination of this process is beyond the scope of this paper and we concentrate hereon on the more readily characterized remote marine environment.

The enhancement of LWP and the initiation of drizzle in the remote marine environment are critical to an understanding of the proposed microphysical process linking gravity wave propagation with POC formation. The raising of the cloud deck as the gravity wave passes leads to a rapid drop in cloud temperature and therefore additional condensation of water vapour in the already saturated cloud layer. This water vapour condenses both onto existing cloud droplets and potentially forms new cloud droplets (subject to availability of CCN), hence increasing cloud LWP, as observed. In this characteristically low CCN remote maritime region (Bretherton et al., 2010; Allen et al., 2011), it might be expected that any additional condensation results in a shift to larger mean droplet size (due to both condensation onto existing droplets and greater collisional coalescence efficiency) and that a proportion of those droplets may become precipitable. Importantly, the LWP observed along the wave fronts in Figure 5a ($100\text{-}140\text{ gm}^{-2}$) is consistent with values known to be sufficient to characterize strongly drizzling Sc in the remote southeastern Pacific (Zuidema et al., 2005) and the detection of co-located drizzle by AMSR-E (see Figure 7b) confirms this. As the wave passes into the negative phase (downward movement of the cloud) and the local temperature rises, remaining small cloud droplets are quickly evaporated to maintain saturation. The period of the observed waves (around one hour) is significantly less than the boundary layer turnover time (~ 3 hours, Wood et al., 2011b) and therefore resupply of moisture to the cloud layer is not fast enough to offset wave-induced thermodynamic changes in relative humidity.

Together, removal of cloud liquid water by precipitation in the upward phase and cloud droplet evaporation in the downward phase, could be expected to lead to large reductions in total water content and hence cloud-clearance. Both the near-LES simulations of Mechem et al. (2011), and a simple parcel model using observed modulation of cloud top height and ECMWF thermodynamic profiles have demonstrated that this is indeed possible over the area and is confirmed here by the GOES-10 satellite observations. For example, consider the following simple thermodynamic calculation for a cloudy air parcel, which is lifted by 250 m (the observed amplitude of the waves). Using typical ECMWF temperature profiles and radiosonde data obtained later in VOCALS-Rex,

such uplift corresponds to a temperature decrease of around 1.5°C. Assuming a cloud top temperature of 13°C (typical of mean values seen in GOES-10 data), this temperature drop for an initially saturated (cloudy) air parcel, corresponds to an additional condensation of 0.9 gm⁻³ of water vapor. If we assume that the initial liquid water content of the unperturbed cloud is ~0.6 gm⁻³ and cloud droplet concentration was 100 cm³ (in line with in situ measurements in remote Sc reported in Bretherton et al., 2009) then the mean droplet size would initially be ~ 20 μm by the following relationship for a cloudy air parcel:

$$\bar{D} = \sqrt[3]{\frac{LWC}{N_d \frac{\pi}{6} \rho_w}} \quad (2)$$

Where D is the mean droplet diameter, LWC is the liquid water content, N_d is the cloud droplet number and ρ_w is the density of liquid water. With the additional condensation induced by the wave uplift, then by (2), the mean droplet size in cloud at the crest of the gravity wave would be ~ 31 μm. This large increase in mean droplet size promotes the development of precipitable droplets by dramatically increased collision and coalescence efficiency and the size calculated in this simple calculation is consistent with cloud top mean droplet sizes expected in drizzling marine Sc (e.g Bott, 1998).

We propose here, based on these observations, that gravity waves are able to initiate drizzle and tip clouds in a predisposed region (of low CCN) into the POC state, shown in the satellite imagery here as an “opening up” of the cloud deck in lines parallel to the phase fronts. An investigation of this process using a cloud resolving model is the subject of a separate study.

A summary of these satellite observations is that the wave fronts shown here propagated for a period of over 36 hours and over a distance in excess of 1500 km, suggesting trapping of wave energy in the troposphere. Having established the changes in observed cloud bulk properties and the microphysical processes that might lead to observed irreversible changes in cloud dynamics at the

mesoscale, we now investigate the source of the gravity waves and briefly discuss the possible reasons for trapping.

4 Sources of gravity wave energy in October 2008

Mesoscale trains of atmospheric gravity waves have been reported many times in the literature, with properties similar to those described here (e.g. Bosart et al 1998). Often, they have been associated with deep convection, but Uccellini and Koch (1987), who presented a summary of thirteen published case studies of such waves, decided that convection was not their main source of energy. They concluded that a common feature in all such events was a jet streak upstream of an upper-level ridge, with the waves found ‘in the exit region of a jet streak and preferentially on its right (anticyclonic shear) side’. Uccellini and Koch were not able to explain the precise mechanism for wave emission, but they suggested shear instability and geostrophic adjustment as the two most likely mechanisms: in the exit region of the jet streak strong departures from nonlinear balance are found, which can cause the emission of gravity waves by geostrophic adjustment. Zhang et al. (2001, 2003) examined this hypothesis in detail for a gravity wave case reported by Bosart et al. (1998), using a simulation of the event with the MM5 mesoscale model. In this case wave initiation occurred just downstream from a region of nonlinear imbalance, itself downstream of an upper-level trough over the Eastern USA. The largest departure from nonlinear balance was found in the tropopause fold beneath the southwesterly branch of the jetstream. The waves generated at upper levels took several hours to reach the surface layer and resulted in one long-lived, large-amplitude gravity wave train that caused hazardous winter weather.

We shall now discuss sources for the wave energy, dealing first with the detailed observational case presented in Section 3 and then with two other cases observed later in October 2008.

4.1. 8 October 2008 case

For the case discussed in Section 3, the wave fronts were first observed near 30°S, 85°W on the afternoon of 7 October 2008. Using the phase speed of the (nondispersive) waves as derived in Section 3 from their track on the cloud field (see Figure 3) and assuming a constant speed and direction we are able to approximately trace back the waves from their initial point of observation in order to diagnose the potential original imbalances that may have acted as a source for the wave energy. Figure 8 shows fields derived from ECMWF operational thermodynamic analyses at 12 UTC on 6 October 2008 (around 36 hours before the waves were first manifest as perturbations to the Sc cloud deck). Figure 8a shows ΔNBE , calculated as described in Section 2.3, at 500 hPa along with the back-traced position of the gravity waves first observed in Figure 1a, marked by a large cross. The dashed line between A and B in Figure 8a defines a line for which a vertical-horizontal-cross-section parallel to the observed wave front is extracted and plotted in Figure 8c and Figure 8d, for ΔNBE and potential vorticity, respectively. Figure 8b shows potential vorticity and horizontal winds on the 340 K isentrope, representative of the sub-tropical upper troposphere and extra-tropical lower stratosphere, therefore illustrating the position of the southern sub-tropical jet-stream. Figure 8b shows a markedly disturbed jet with three breaking Rossby waves between 140° W and 60° W. The point of interest here, corresponding to the black cross in Figure 8a, is around 95° W, 36° S, just downwind from a ridge at 340K. This breaking Rossby wave resulted in a tropopause fold, shown in Figure 8d, which coincided with the large negative NBE residual vertical profile at 36° S (dark blue contours) seen in Figure 8c extending from 200 to 800 hPa. This large negative NBE residual results from convergence occurring in the equatorward branch of the jet stream downstream from the ridge, following the rapid increase in absolute vorticity along the flow. A full animated sequence of the ECMWF fields displayed in Figure 8 across October 2008 is provided as a supplement to this paper and illustrates more clearly the movement of the breaking Rossby waves across the SEP.

Temperature and humidity profiles from the ECMWF analyses along the path of the gravity wave trains showed a moist, neutrally stable boundary layer capped by a very prominent inversion ($\Delta\theta \sim 5$

K in 200 m). This layer was too thin to support the gravity waves observed here, which would have propagated into the stable layer above (Brunt-Vaisala frequency $N \sim 0.01 \text{ s}^{-1}$). However, at the level of the inversion (or cloud top) the waves in fact propagated horizontally for around 2000 km without observable loss of amplitude. Linear, steady wave ducting by critical layers is one mechanism proposed in the literature for trapping gravity waves in the vertical (Lindzen and Tung, 1976). The non-dispersive nature of the waves would suggest a vertical wavelength of order 10 km. Indeed, there were critical layers in the upper troposphere along much of the path of the waves according to the ECMWF analyses, but the model static stability suggests that such layers would absorb rather than trap the wave energy. As we do not have detailed vertical profiles of static stability we cannot rule out the Lindzen and Tung mechanism here but it does not appear to be a strong candidate.

Short of some mechanism for reflecting the wave energy at the tropopause, we must consider the possibilities that the observed undulations of the Sc deck are either a time-dependent wave with a complex, non-linear propagation, or result from a mechanism for wave amplification compensating for radiation losses. One such mechanism might arise from an interaction between the Sc deck and the wave, whereby subsidence across the inversion is affected by the vertical displacement associated with the wave.

The limited vertical resolution of the ECMWF analyses, and the lack of in-situ profiles in the region at this time, preclude a detailed investigation of wave propagation. High-resolution model simulations are currently under way to determine whether the waves were predictable, given the large-scale flow pattern. The evidence in this section however clearly points to waves being generated by geostrophic adjustment around the subtropical jetstream, followed by horizontal propagation in the free troposphere for around 2000 km.

4.2. 11 October 2008 case

Figure 9 shows the same fields as Figure 8, here at 0600 UTC on 10 October 2008, corresponding to a gravity wave train that was first observed in satellite imagery over the SEP near 82°W, 21.5°S at 1528 UTC, 11 October 2008 (not shown). In this case, the observed gravity wave traces back to a region of negative Δ NBE just upstream of the point where a midlatitude trough extends north towards the subtropical jetstream.

4.3. 27 October 2008 case

Figure 10 shows the same fields as Figure 8, here at 0600 UTC on 27 October 2008, corresponding to a gravity wave train that was first observed in satellite imagery over the SEP near 80°W, 34°S at 0528 UTC, 27 October 2008 (not shown). In this case, the origin of the waves traces back to a point at 30°S, 82°W, where we see a marked anticyclonically-breaking (LC1 type) Rossby wave in Figure 10b. Similar to the 8 October case, we see a profile of large negative Δ NBE at this location (Figure 10c) coinciding with the tropopause fold.

4.4. Common sources

In all three cases observed in October 2008, the observed gravity wave trains trace back to a region of large negative residual NBE and hence areas of flow divergence. This points to a gravity wave energy source by geostrophic adjustment. For the 8 October and 27 October cases, these areas of residual NBE are tropopause folds associated with LC2 and LC1 Rossby wave breaking, respectively, along the subtropical jetstream. For the 11 October case, the Rossby wave appears poleward of the STJ – i.e. in the polar jetstream. Satellite imagery and ECMWF fields were also examined for November 2008 - at times when gravity waves were not observed in GOES-10 imagery, there was neither evidence of nearby Rossby wave activity nor centres of large negative Δ NBE. Indeed there were no further gravity waves observed in the imagery during the VOCALS-REx campaign or throughout November 2008, a period characterised by a quiescent STJ (Toniazzi et al., 2011).

5. Conclusions

This study has demonstrated a previously unknown role for atmospheric gravity waves in the South East Pacific region by their ability to modulate cloud radiative and dynamical properties over a wide area. Using satellite imagery and satellite-retrieved cloud bulk properties during October 2008 over the SEP, we have illustrated the horizontal propagation of a series of gravity wave trains by their influence on the stratocumulus cloud deck capping the local marine boundary layer. The waves were observed as a non-dispersive periodic modulation of retrieved cloud top height by up to 500 m peak-to-trough during a case study of waves observed on 8 October 2008, whilst the horizontal direction of wave propagation was perpendicular to the synoptic boundary layer flow. The waves appeared to originate near 30°S, 85°W and were initiated for a 2-hour period beginning at midday on 7 October 2008, propagating along a vector directed approximately northeastward toward the Peruvian Coast (15°S, 70°W) over the following 36 hours, covering a distance in excess of 1500 km. During that time, the gravity waves were observed to affect both reversible and non-reversible changes in cloud radiative properties and cloud dynamics such that POCs developed in the troughs of passing gravity wave fronts. The POCs were observed to form in regions with high background LWP and the gravity waves were observed to enhance this LWP further, consistent with an expected increase in precipitation rate in this low CCN environment. The increase in precipitation rate, by whatever means, is a mechanism common to previous studies of POC development in the SEP.

Two additional cases (11 October and 27 October 2008) of gravity wave propagation were observed in satellite imagery of the SEP later in October 2008. Lagrangian back-tracking from their point of manifestation on the cloud deck for both these waves and those examined in detail for the 8 October case, show that waves originated in areas displaying large negative residual to the nonlinear balance equation, which were associated with Rossby waves propagating along the subtropical and polar jetstreams. We propose here that these gravity waves were generated by geostrophic adjustment

around the jetstreams.. Although this is consistent with mesoscale gravity wave events previously recorded in the literature, the waves in this case propagated equatorward rather than poleward. This occurred because of a wave duct, probably caused by a critical layer for the waves embedded in a region of low static stability on the equatorward side of the subtropical jetstream.

This case study demonstrates that gravity waves and their impacts on stratocumulus thermodynamics in the SEP are one formative mechanism for POCs in the region and serves to demonstrate and highlight the important effects that gravity waves propagating in the troposphere can have on cloud radiative properties (and hence surface radiation budgets) over a significant spatial extent. These results also emphasise the importance of synoptic influence on stratocumulus covered marine boundary layers through changes to the liquid water path and hence precipitation rate.

Acknowledgements

The UK element of the VOCALS-REx campaign was funded by a Natural Environment Research Council consortium grant (Grant ref: NE/F019874/1). We thank the European Centre for Medium-Range Weather Forecasts (ECMWF) for operational reanalysis data, provided by the British Atmospheric Data Centre (available from: <http://badc.nerc.ac.uk/data/ecmwf-op/>). Yuter and Burleyson were supported by U.S. National Oceanic and Atmospheric Administration grant GC09-252b and U.S. National Aeronautical and Space Administration grants NNX10AP43H and NNX11AE98G. Support for developing the GOES-10 data products was provided by the Department of Energy ARM Program and the NASA Modelling, Analysis, and Prediction Program.

References

Allen, G., Coe, H., Clarke, A., Bretherton, C., Wood, R., Abel, S. J., Barrett, P., Brown, P., George, R., Freitag, S., McNaughton, C., Howell, S., Shank, L., Kapustin, V., Brekhovskikh, V., Kleinman, L., Lee, Y.-N., Springston, S., Toniazzo, T., Krejci, R., Fochesatto, J., Shaw, G., Krecl, P., Brooks, B., McMeeking, G., Bower, K. N., Williams, P. I., Crosier, J., Crawford I., Connolly, P., Allan, J. D., Covert, D., Bandy, A. R., Russell, L. M., Trembath, J., Bart, M., McQuaid, J. B., Wang, J., and Chand, D.: South East Pacific atmospheric composition and variability sampled along 20° S during VOCALS-REx, *Atmos. Chem. Phys.*, 11, 5237-5262, doi:10.5194/acp-11-5237-2011

Bosart, L. F., Bracken, W. E. and Seimon, A., A study of cyclone mesoscale structure with emphasis on a large-amplitude inertia-gravity wave. *Mon. Wea. Rev.* **126**, 1497-1527, 1998.

Bott, A.: A flux method for the numerical solution of the stochastic collection equation, 55, pp2284-2293, *J. Aero. Sci.*, 1998.

Bretherton, C. S., Uttal, T., Fairall, C.W., Yuter, S. E., Weller, R. A., Baumgardner, D., Comstock, K., and Wood, R.: The EPIC 2001 stratocumulus study, *Bull. Am. Meteor. Soc.*, **85**, 967–977, 2004.

Bretherton, C. S., Wood, R., George, R. C., Leon, D., Allen, G., and Zheng, X.: Southeast Pacific stratocumulus clouds, precipitation and boundary layer structure sampled along 20° S during VOCALS-REx, *Atmos. Chem. Phys.*, 10, 10639–10654, doi:10.5194/acp-10-10639-2010, 2010.

Comstock, K., Bretherton, C. S., and Yuter, S.: Mesoscale variability and drizzle in Southeast Pacific stratocumulus, *J. Atmos. Sci.*, **62**, 3792–3807, 2005.

Comstock, K., Yuter, S. E., Wood, R., and Bretherton, C. S.: The three dimensional structure and kinematics of drizzling stratocumulus, *Mon. Wea. Rev.*, **135**, 3767–3784, 2007.

de Szoeke, S. P., Yuter, S. E., Zuidema, P., Fairall, C. W., and Brewer, W. A.: Ship-based observation of drizzling stratocumulus clouds from EPIC to VOCALS. *CLIVAR Exchanges*, **15**, 11-13, 2010

George, R. C. and Wood, R.: Subseasonal variability of low cloud radiative properties over the southeast Pacific Ocean, *Atmos. Chem. Phys.*, 10, 4047-4063, doi:10.5194/acp-10-4047-2010, 2010.

Haag, W. and Karcher, B.: The impact of aerosols and gravity waves on cirrus clouds at midlatitudes, *J. Geophys. Res.*, **109**, D12202, doi:10.1029/2004JD004579, 2004.

Knippertz, P., Chagnon, J. M., Foster, A.; Lathouwers, L., Marsham, J. H., Methven, J; Parker, D. J.: Research flight observations of a prefrontal gravity wave near the southwestern UK, *WEATHER*, 65, pp.293-297, 2010.

Knippertz, P., Chagnon, J.M. Foster, A., Lathouwers, L., Marsham, J. H., Methven, J., Parker, D., Research flight observations of a prefrontal gravity wave near the southwestern UK, *Weather*, **65**, , 293–297, 2010.

Koch, S. E., and O' Handley, C.: Operational forecasting and detection of mesoscale gravity waves, *Weather and Forecasting*, 12,253-281, 1997.

Koch, S. E., Hamilton, D., Kramer, D., and Langmaid, A.: Mesoscale dynamics in the Palm Sunday tornado outbreak, *Mon. Weather Rev.*, 126,203 1-2060, 1998.

Lindzen, R. S. and Tung, K. K.: Banded convective activity and ducted gravity waves. *Mon. Wea. Rev.* **104**, 1602-1617, 1976.

McFarlane, N. A.: The effect of orographically excited gravity wave drag on the general circulation of the lower stratosphere and troposphere, *J. Atmos. Sci.*, **44**, 1775-1800, 1978.

McLandress, C: On the importance of gravity waves in the middle atmosphere and their parameterization in general circulation models. *J. Atmos. Solar-Terr. Phys.*, **60**, 1357-1383, 1998.

Mechem, D. B., Yuter, S. E. and deSzoek, S. P.: Thermodynamic and aerosol controls in southeast Pacific stratocumulus, *J. Atmos. Sci.*, Submitted, 2011

Meehl, G. A., Stocker, T. F., Collins, W. D., Friedlingstein, P., Gaye, A. T., Gregory, J. M., Kitoh, A., Knutti, R., Murphy, J. M., Noda, A., Raper, S. C. B., Watterson, I. G., Weaver, A. J., and Zhao, Z.-C.: Global climate projections, in: *Climate Change 2007: The Physical Science Basis. Contribution of Working Group I to the Fourth Assessment Report of the Intergovernmental Panel on Climate Change*, edited by: Solomon, S., Qin, D., Manning, M., Chen, Z., Marquis, M., Averyt, K. B., Tignor, M., and Miller, H. L., Cambridge University Press, Cambridge, UK and New York, NY, USA, 2007.

Menzel, W. P., and Purdom, J. F. Y.: Introducing GOES I: The first of a new generation of Geostationary Operational Environmental Satellites, *Bull. Am. Meteorol. Soc.*, **75**, 757-781, 1994.

Miller, M. A., and S. E. Yuter, 2011: Detection and characterization of drizzle cells within marine stratocumulus using AMSR-E 89 GHz passive microwave measurements. *J. Geophys. Res.*, submitted June 2011.

Minnis, P., et al: CERES Edition-2 cloud property retrievals using TRMM VIRS and Terra and Aqua MODIS data, Part I: Algorithms. *IEEE Trans. Geosci. Remote Sens.*, **49**, 11, doi: 10.1109/TGRS.2011.2144601, 2011.

Moore, J. T., and Abeling, W. A.: A diagnostic of unbalanced flow in upper levels during the AVE-SESAME I period. *Mon. Weather Rev.*, 116,2425-2436, 1988.

Rahn, D. A., R. Garreaud, J. Rutllant, 2011: The low-level atmospheric circulation near Tongoy Bay / point Lengua de Vaca (Chilean coast, 30°S). *Mon. Wea. Rev.*, in press., 2011.

Randall, D. A., Wood, R. A., Bony, S., Colman, R., Fichefet, T., Fyfe, J., Kattsov, V., Pitman, A., Shukla, J., Srinivasan, J., Stouffer, R. J., Sumi, A., and Taylor, K. E.: Climate models and their evaluation, in: *Climate Change 2007: the Physical Science Basis, Contribution of Working Group I to the Fourth Assessment Report of the Intergovernmental Panel on Climate Change*, edited by: Solomon, S., Qin, D., Manning, M., Chen, Z., Marquis, M., Averyt, K. B., Tignor, M., and Miller, H. L., Cambridge University Press, Cambridge, UK and New York, NY, USA, 2007.

Stevens, B., Vali, G., Comstock, K., Wood, R., VanZanten, M., Austin, P. H., Bretherton, C. S., and Lenschow, D. H.: Pockets of Open Cells (POCs) and drizzle in marine stratocumulus, *Bull. Am. Meteor. Soc.*, **86**, 51–57, 2005.

Toniazzo, T. Abel, S. J., Wood, R. A., Mechoso, S. R., Allen, G., and Shaffrey, L. C.: Large-scale and synoptic meteorology in the south-east Pacific during the observations campaign VOCALS-REx in Spring 2008, *Atmos. Chem. Phys.*, **11**, 4977-5009, 2011

Thorncroft, C. D., B. J. Hoskins and M. E. McIntyre: Two paradigms of baroclinic-wave life-cycle behaviour. *Quart. J. Roy. Meteor. Soc.*, **119**, 17-55, 1993.

Uccellini, L. W. and Koch, S. E.: The synoptic setting and possible energy sources for mesoscale wave disturbances. *Mon. Wea. Rev.*, **115**, 721-729, 1987.

Wang, H., Feingold, G., Wood, R. and Kazil, J.: Modelling microphysical and meteorological controls on precipitation and cloud cellular structures in Southeast Pacific stratocumulus, *Atmos. Chem. Phys.*, **10**, 6347-6362, 2010.

Wood, R., Comstock, K. K., Bretherton, C. S., Cornish, C., Tomlinson, J., Collins, D. R., and Fairall, C.: Open cellular structure in marine stratocumulus sheets, *J. Geophys. Res.*, **113**, doi:10.1029/2007JD009 596, 2008.

Wood, R., Bretherton, C. S., Leon, D., Clarke, A. D., Zuidema, P., Allen, G., and Coe, H.: An aircraft case study of the spatial transition from closed to open mesoscale cellular convection, *Atmos. Chem. Phys.*, **11**, 2341-2370, 2011a

Wood, R., Allen, G., et al., The VAMOS Ocean-Cloud-Atmosphere-Land Study Regional Experiment (VOCALSREx): goals, platforms, and field operations, *Atmos. Chem. Phys. DiScss.*, *Atmos. Chem. Phys.*, **11**, 627-654, 2011b.

Zdunkowski, W. and Bott, A.: Dynamics of the atmosphere, Cambridge University Press, Cambridge, UK, 2003.

Zack, J. W. and Kaplan, M. L.; Numerical simulations of the subsynoptic features associated with the AVE-SESAME I case. Part I: The pre-convective environment. *Mon. Weather Rev.*, 115,2367-2394, 1987

Zhang, F., Koch, S. E., Davis, C. A. and Kaplan, M. L.: Wavelet analysis and the governing dynamics of a large-amplitude mesoscale gravity-wave event along the East Coast of the United States, *Quart. J. Roy. Meteorol. Soc.*, **127**, 2209-2245, 2001.

Zhang, F., Koch, S. E. and Kaplan, M. L.: Numerical simulations of a large-amplitude mesoscale gravity wave event, *Meteorol. Atmos. Phys.*, **84**, 199-216, 2003.

Zuidema, P., Westwater, E. R., Fairall, C., and Hazen, D.: Ship-based liquid water path estimates in marine stratocumulus, *J. Geophys. Res.*, 110, D20206, doi:10.1029/2005JD005833, 2005.

Zdunokowski, W., and Bott, A.: Dynamics of the atmosphere: A course in theoretical meteorology, Cambridge University Press, 2003.

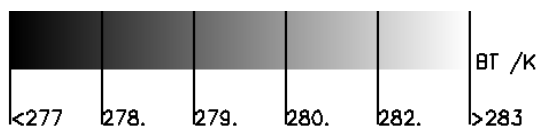
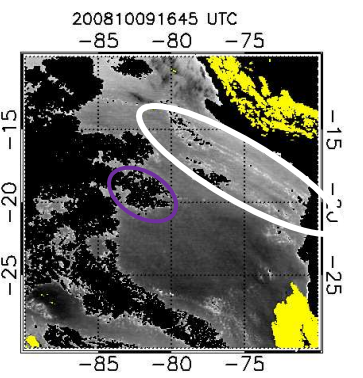
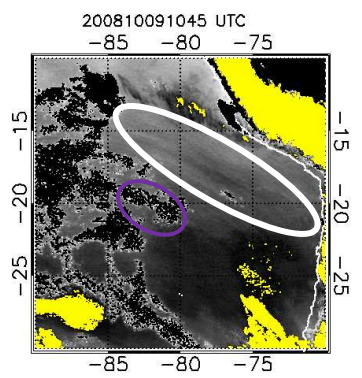
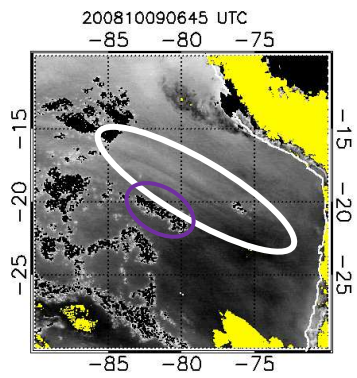
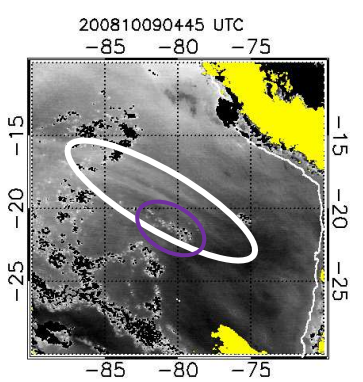
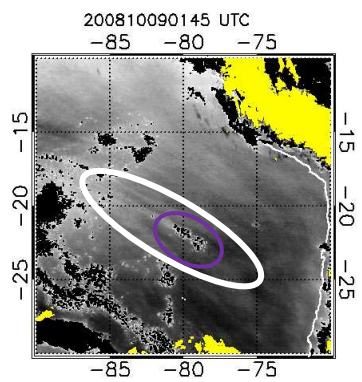
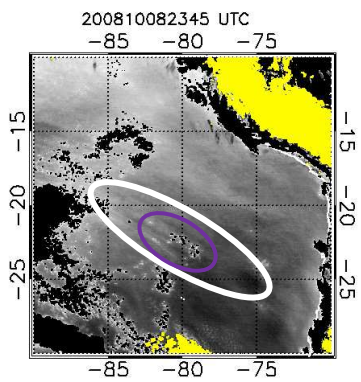
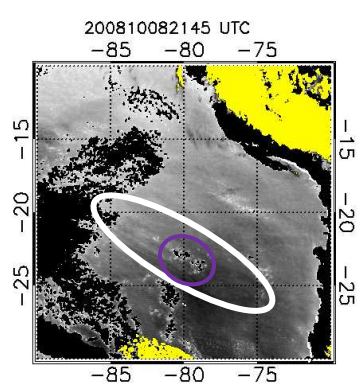
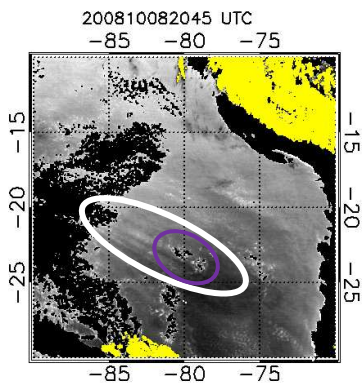
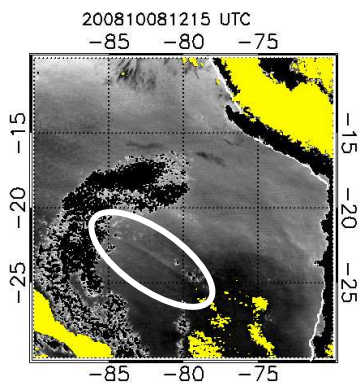
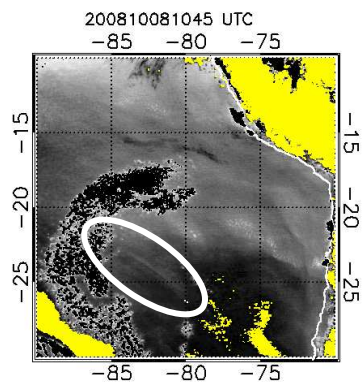
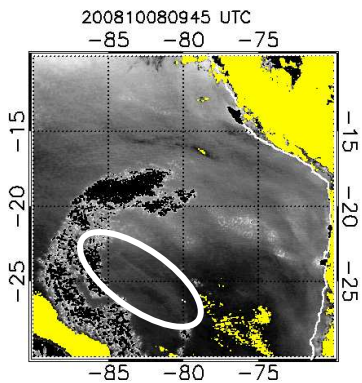
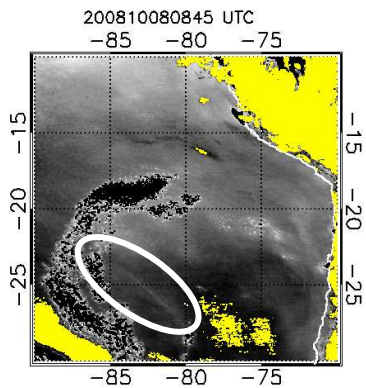


Figure 1. Time sequence (see time labels for each panel) of GOES-10 infrared window brightness temperature across the period 0845 UTC, 8 October 2008 to 1645 UTC, 10 October 2008. The sequence shows the progression of a gravity wave front highlighted by a white ellipse, with a developing POC feature encircled in a purple ellipse (where observed).

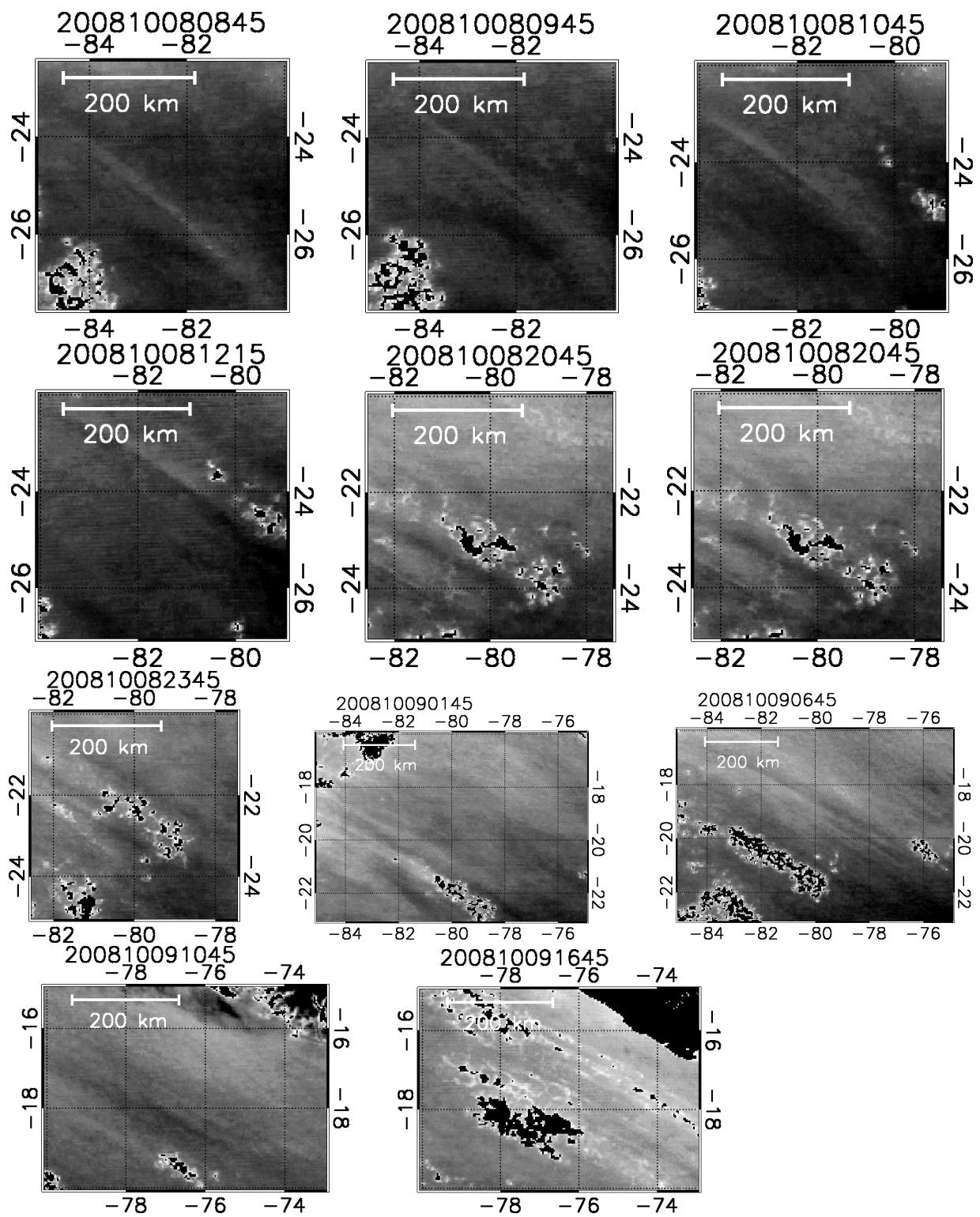


Figure 2 Magnified images of the time sequence (see time labels for each panel) of GOES-10 IRW brightness temperatures across the period 0845 UTC, 8 October 2008 to 1645 UTC, 10 October 2008, presented in Figure 1.

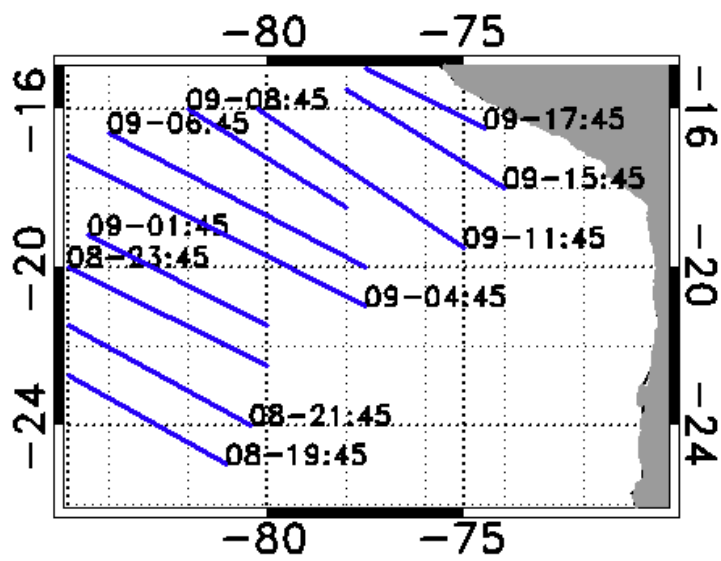


Figure 3 – A composite schematic showing the position and extent of gravity wave fronts (in blue) in the South East Pacific as observed in GOES-10 imagery. The label for each wavefront gives the day in October 2008 followed by Universal Time.

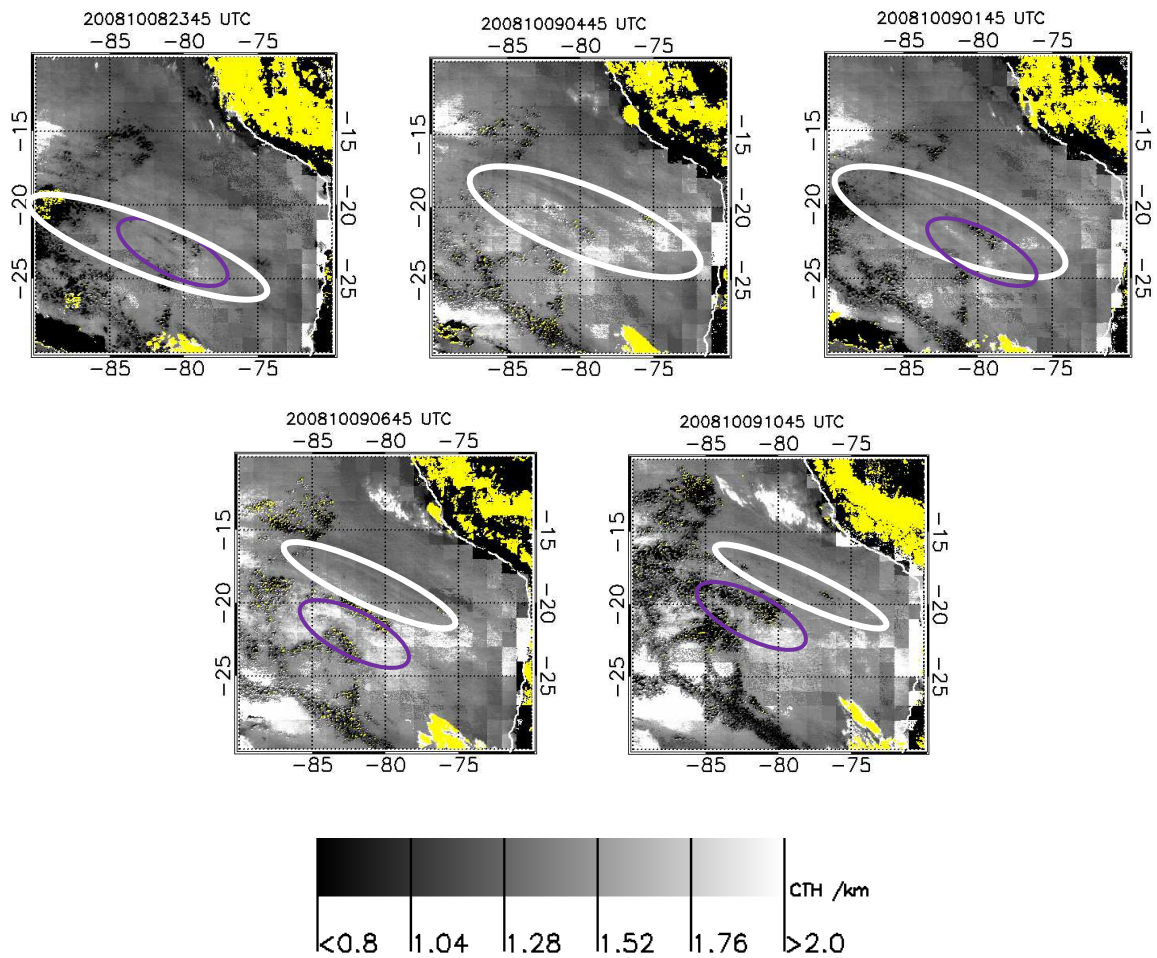


Figure 4. Time sequence (see time labels for each panel) of selected GOES-10 IRW-retrieved cloud top height (CTH) as indicated by the grayscale bar across the period 2345 UTC, 8 October 2008 to 1045 UTC, 10 October 2008. The sequence shows the progression of a gravity wave front highlighted by a white ellipse, with a mature POC feature in the purple ellipses (where observed).

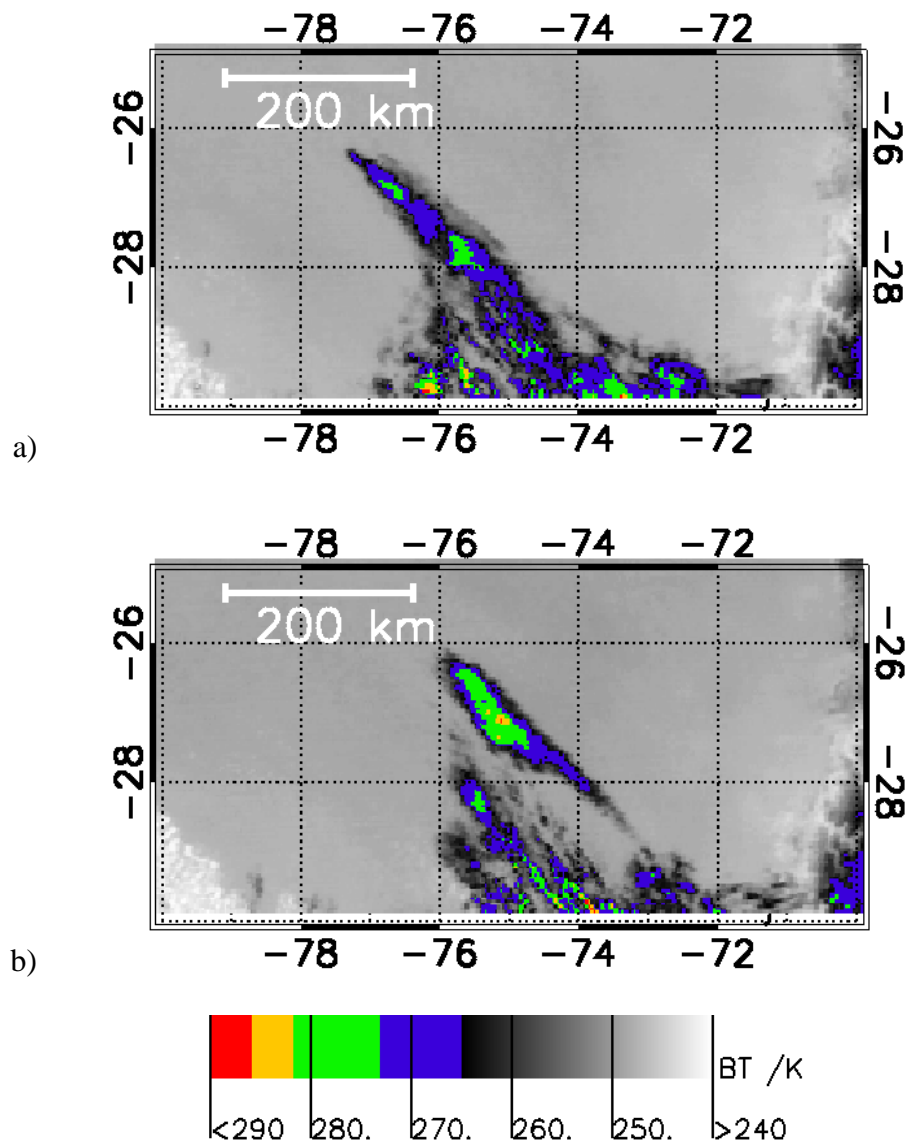


Figure 5 Cloud brightness temperature field retrieved from GOES-10 radiances in the region 30 to 25 ° S, 80 ° W to 70 ° W and colour-scaled as indicated for a) 0828 UTC; and b)0958 UTC, on 9 October 2008.

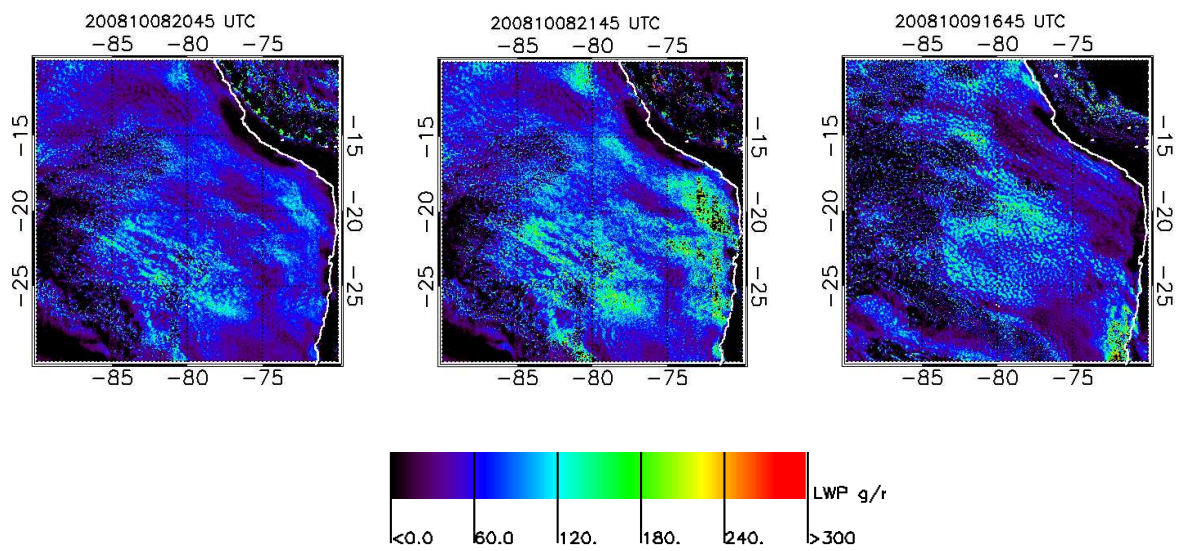


Figure 6. Time sequence (see time labels for each panel) of selected GOES-10 retrieved liquid water path (LWP) as scaled. Only those LWP retrievals which were possible in daylight hours are presented.

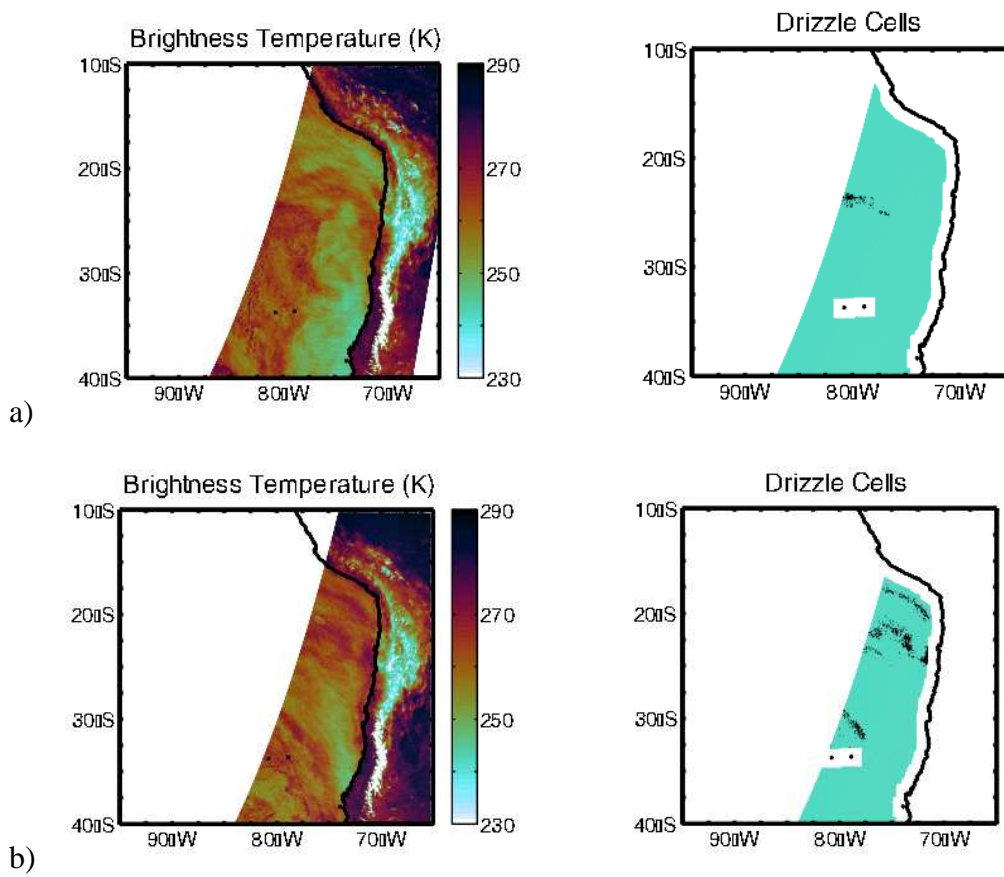


Figure 7. Brightness temperature swaths (left panels) retrieved at 89 GHz from AMSR-E overpasses, and strong drizzle detection (black area in right panels) at: a) 0540 UTC, 7 October 2008; b) 0528 UTC 9 October 2008. Note: The black dots inside white squares near 33 ° S, 88 W, are two islands, which are masked for the purposes of the drizzle retrieval algorithm.

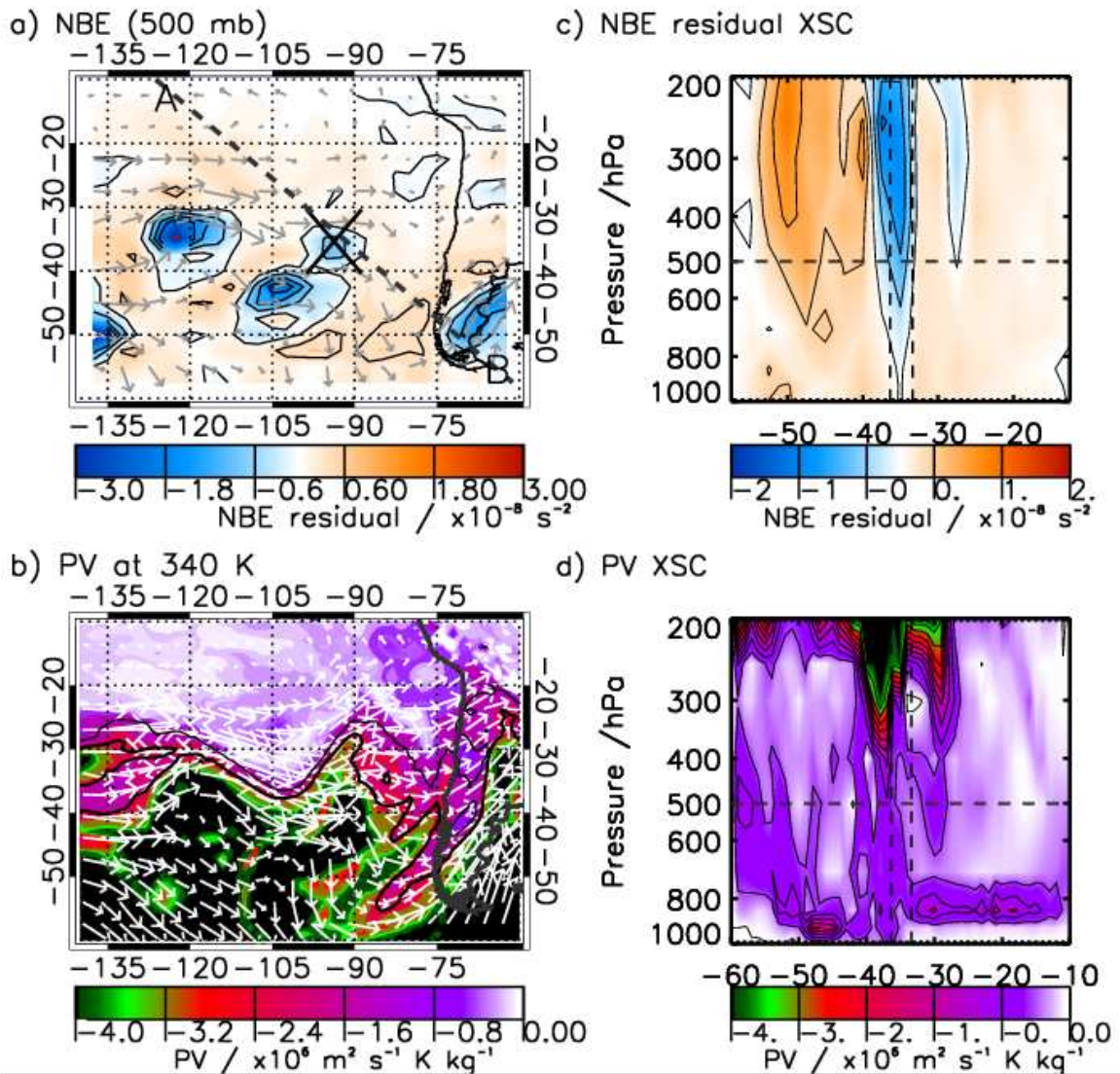


Figure 8. Thermodynamic operational analysis and derived fields from the ECMWF IFS at 1200 UTC on 6 October 2008 for: a) Residual of the NBE (colour-scale) and scaled horizontal winds (grey arrows) evaluated at 500 hPa ; b) Potential vorticity (colour-scale) evaluated on the 340 K isentropic surface with scaled horizontal wind arrows (white); c) Vertical-horizontal cross-section of residual of NBE, extracted along the dashed line of panel a, marked between AB; and d) Cross-section of potential vorticity along the same line. The abscissa in panels c and d is the latitude along the cross-section. The cross in panel a marks the mid-point of the gravity wave packet observed at 0845 UTC on 8 October 2008, projected back in time to 1200 UTC on 6 October using the measured phase speed. The dashed lines on panel c represent a line along the 500 hPa level (for reference to panel a) and the latitudinal range of the back-projected wave-front, respectively.

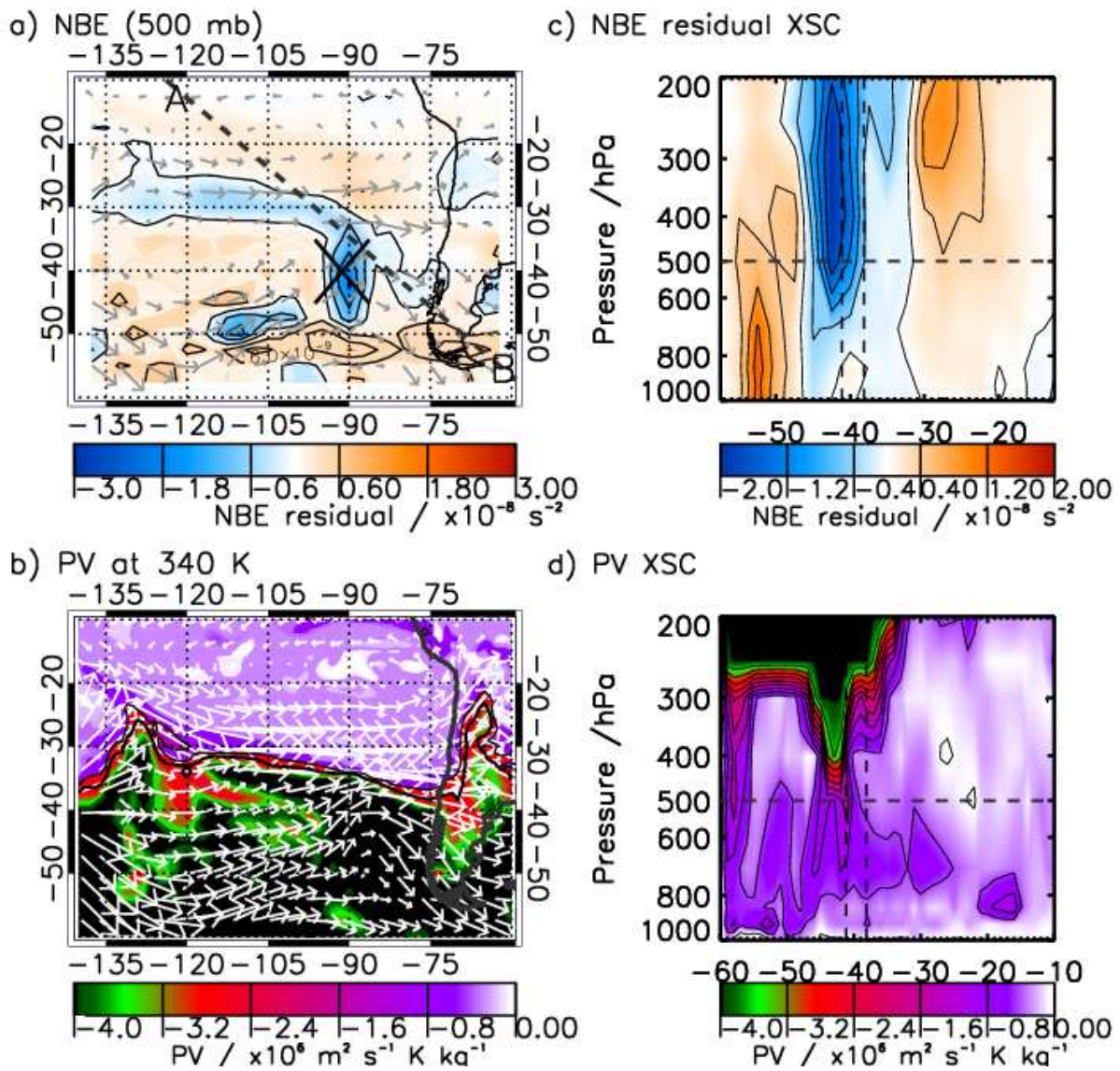


Figure 9. Same as Figure 8 for 0600 UTC on 10 October 2008, with the black cross in panel a marking the mid-point of the backward-traced gravity wave front observed at 1528 UTC on 11 October 2008.

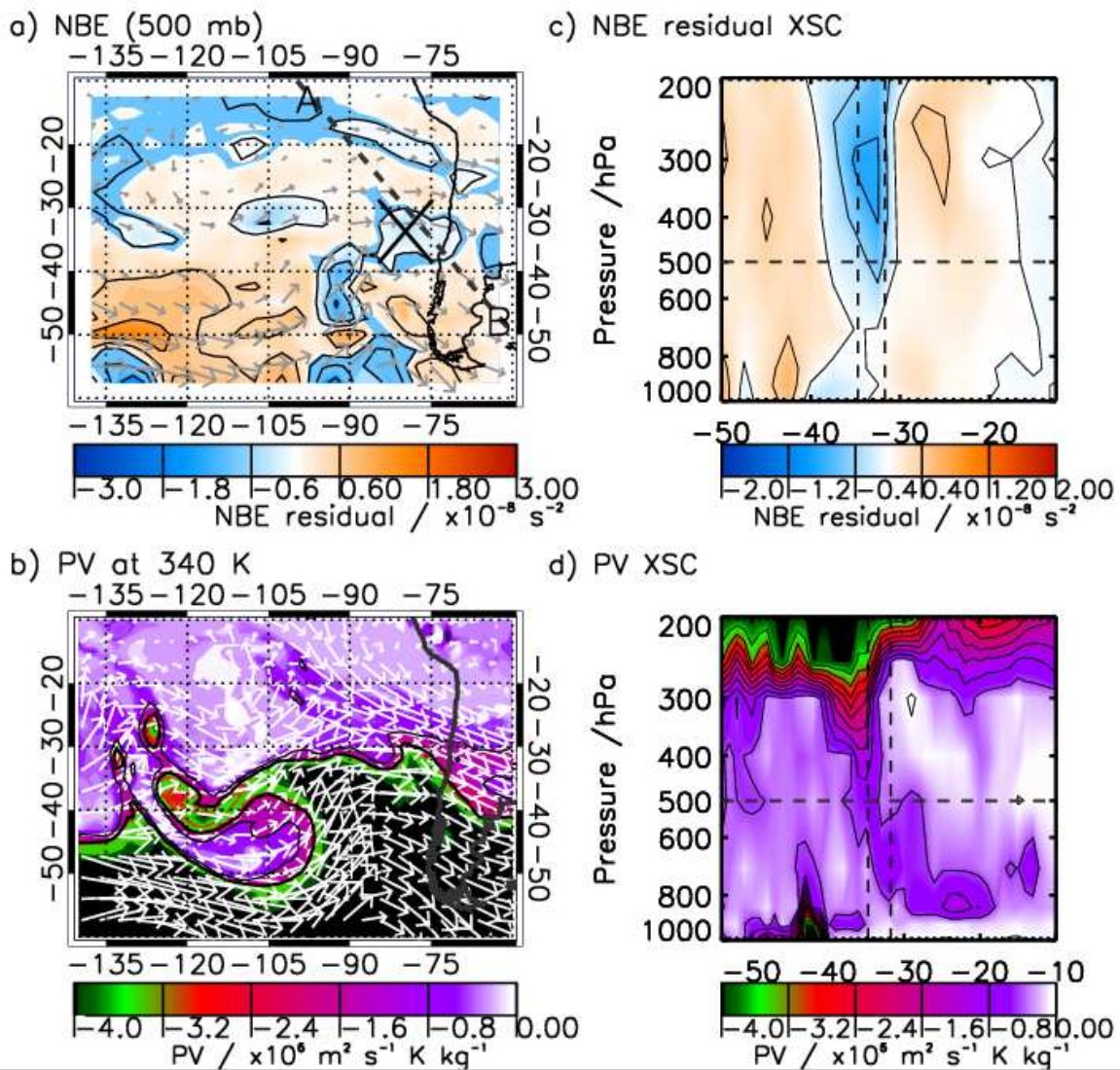


Figure 10. Same as Figure 8 caption for 0600 UTC on 27 October 2008, with the exception that the black cross in panel a marks the mid-point of the backward-traced gravity wave front observed at 0528 UTC on 27 October 2008.